

# Exploring Mechanisms of Lang Qing Ata in Non-Alcoholic Steatohepatitis Based on Metabolomics, Network Pharmacological Analysis, and Experimental Validation

Shupe Li<sup>1,\*</sup>, Hanlong Zhu<sup>2,\*</sup>, Qi Zhai<sup>2,\*</sup>, Yu Hou<sup>2,\*</sup>, Ya Yang<sup>2,\*</sup>, Haifeng Lan<sup>3</sup>, Mingzuo Jiang<sup>2</sup>, Ji Xuan<sup>1,2</sup>

<sup>1</sup>Department of Gastroenterology, Jinling Clinical Medical College, Nanjing University of Chinese Medicine, Nanjing, Jiangsu, People's Republic of China; <sup>2</sup>Department of Gastroenterology and Hepatology, Jinling Hospital, Affiliated Hospital of Medical School, Nanjing University, Nanjing, Jiangsu, People's Republic of China; <sup>3</sup>Department of Gastroenterology, Jinling Clinical Medical College, Nanjing Medical University, Nanjing, Jiangsu, People's Republic of China

\*These authors contributed equally to this work

Correspondence: Ji Xuan, Department of Gastroenterology and Hepatology, Jinling Clinical Medical College, Nanjing University of Chinese Medicine, Nanjing, Jiangsu Province, 210002, People's Republic of China, Tel +86 13851940720, Email xuanji@nju.edu.cn; Mingzuo Jiang, Department of Gastroenterology and Hepatology, Jinling Hospital, Medical School of Nanjing University, Nanjing, Jiangsu Province, 210002, People's Republic of China, Email JMZ199111@163.com

**Background:** Non-alcoholic steatohepatitis (NASH), as a progressive form of Non-alcoholic fatty liver disease (NAFLD), poses a significant threat to human health as a prevalent and common condition, with a lack of safe and effective therapeutic options. However, the therapeutic effects and potential mechanisms of Lang Qing Ata (LQAtta) against NASH remain elusive.

**Materials and Methods:** The components of LQAtta were identified using Ultra-High Performance Liquid Chromatography-Tandem Mass Spectrometry (UHPLC-MS/MS). Subsequently, we employed network construction and analysis approaches within the field of network pharmacology. By integrating known databases and target prediction algorithms, which encompassed database-based target prediction, protein-protein interaction networks, as well as Gene Ontology (GO) and Kyoto Encyclopedia of Genes and Genomes (KEGG) pathway enrichment analyses, we unveiled the potential key targets and signaling pathways that these bioactive components might engage with. These discoveries were further validated in subsequent mouse models. An HFHC-induced NASH mouse model was used to validate the therapeutic effects and potential mechanisms of LQAtta on NASH.

**Results:** From the UHPLC-MS/MS analysis of LQAtta, a total of 1518 chemical components were identified, with 106 of them being absorbed into the bloodstream. Additionally, based on the acquisition of targets from both LQAtta and the NASH database, a total of 160 common targets were screened. KEGG enrichment analysis indicated that LQAtta may alleviate NASH by modulating pathways such as the Toll-like receptor signaling pathway, the NF- $\kappa$ B signaling pathway, and inflammation-related pathways. In vivo experimental results demonstrated that LQAtta could alleviate liver injury, steatosis, and inflammation induced by NASH, thereby slowing down the disease process. Additionally, LQAtta inhibited the expression and phosphorylation of NF- $\kappa$ B protein, playing a role in preventing NASH.

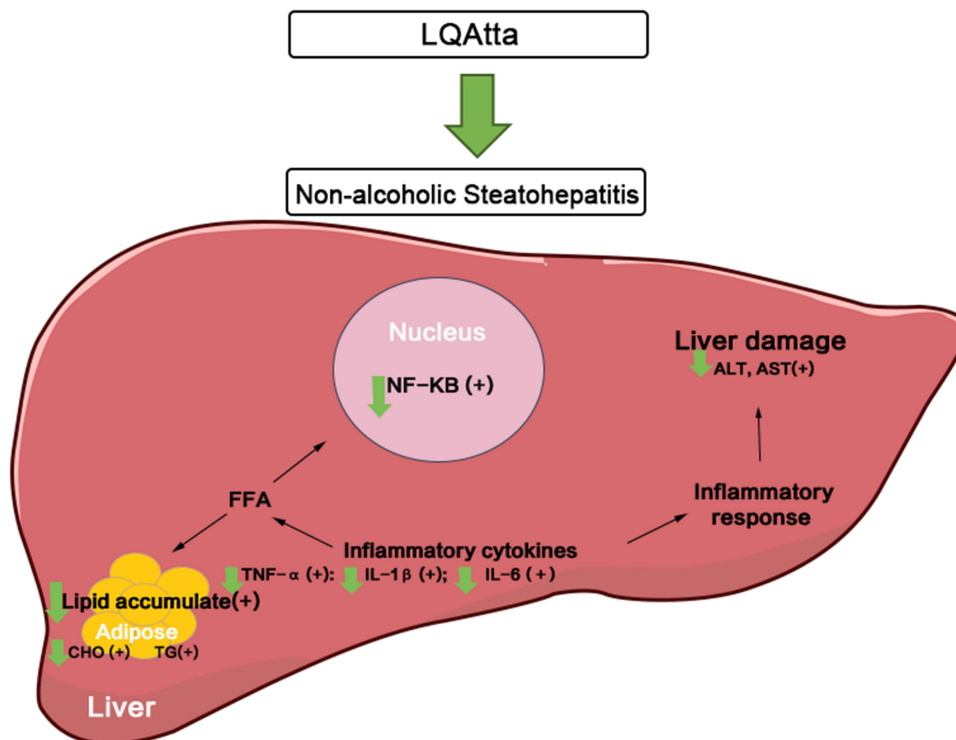
**Conclusion:** In this study, the combination of mass spectrometry analysis, network pharmacology, and animal experiments preliminarily elucidated the potential of LQAtta to treat NASH through NF- $\kappa$ B pathways.

**Keywords:** NAFLD, NASH, network pharmacological analysis, metabolomics, Chinese herbal medicine

## Introduction

Non-alcoholic fatty liver disease (NAFLD) is a common condition characterized by hepatic steatosis or significant lipid deposition in the hepatocytes. This is without influence from other lipid sources including some drugs, high alcohol intake, or specific genetic diseases.<sup>1-3</sup> A particular variant of this disease is non-alcoholic steatohepatitis (NASH) which

## Graphical Abstract



is defined clinically and pathologically by the combination of steatosis, inflammation, and fibrosis as a consequence of fat overload in hepatocytes. NASH is the most advanced and potentially irreversible stage of NAFLD that is characterized by the development of more severe complications such as liver fibrosis, cirrhosis, and even hepatocellular carcinoma.<sup>4</sup> This condition often occurs with other metabolic diseases, such as type 2 diabetes, obesity, and insulin resistance, which increase the risk of inflammation in the body.<sup>5,6</sup> Hence, the prevalence of cardiovascular diseases and malignancies is high amongst individuals who have been diagnosed with NASH, which in turn increases the mortality rate of such patients.<sup>7-10</sup>

Nuclear factor-kappa B (NF-κB) is a protein complex and an essential atomic transcription factor in cells, participating in inflammatory responses, immune responses, regulating cell apoptosis, and stress responses. It serves as the most significant regulator of inflammation.<sup>11</sup> The NF-κB protein complex is composed of five distinct subunits: The major family members are: RelA (p65), NF-κB (p100/p52), NF-κB1 (p105/p50), RelB, and cRel.<sup>12</sup> Because the IκB kinase (IKK) complex should be activated for the initiation of the canonical signaling pathway leading to NF-κB activation.<sup>13,14</sup> In NASH the NF-κB pathway is upregulated and in many cases, there is an increase in the levels of proinflammatory cytokines like IL-6, TNF-α,<sup>15</sup> and IL-1β<sup>13,16</sup> that are frequently found in obese patients. Therefore, this signaling plays a critical role in the advancement of NASH.<sup>17</sup> In their preliminary basic research on liver fibrosis, Xuan et al<sup>18</sup> found that LQAtta can alleviate liver fibrosis by inhibiting the expression of p38 and NF-κB.

Lang Qing Ata (LQAtta), also known as Hua Gan Tong Luo Fang, is a renowned empirical prescription in Tibetan medicine for treating liver diseases. This formula possesses the efficacy of reducing body heat and detoxifying, as well as soothing the liver and promoting bile flow. It has been transmitted for over five hundred years and constitutes an integral part of China's ethnic medicine. In Traditional Chinese Medicine (TCM) theory, the etiology of NASH is complex, often attributed to dietary indulgence, emotional injury, excessive strain or idleness, leading to dysfunction of the liver, spleen, and kidney, internal generation of phlegm-dampness, and blood stasis obstructing the liver meridians.<sup>19</sup> Since 2007, under the funding of Jiangsu Provincial Science and Technology Department (NO.BS2007089), Professor Tian

Yaozhou's<sup>18</sup> research team has collaborated with Lhasa Plateau Biology Research Institute to jointly develop the Tibetan medicine Lang Qing Ata (Hua Gan Tong Luo Fang). Through relentless efforts, the pharmacological and toxicological evaluations of this medicine have been completed, and it has successfully obtained an SFDA clinical approval (Batch Number: 2012L00847) as well as a national invention patent (Patent Application Number: 201010187089.9). Currently, it is being used in clinical treatment. The research team<sup>18,19</sup> has previously published multiple Chinese and English papers, fully demonstrating the significant effects of LQAtta in treating liver cirrhosis and fibrosis, improving liver function, protecting hepatocytes, and repairing liver tissue. In clinical practice for treating liver fibrosis, we found that this formula exhibits particularly prominent efficacy in treating liver fibrosis caused by NASH. We focused on NASH not only because previous studies have shown that LQAtta is effective against hepatic fibrosis caused by NASH, but also based on the close pathological relationship between NASH and hepatic fibrosis. NASH is a progressive liver disease. Its persistent inflammatory response and oxidative stress can lead to excessive deposition of the extracellular matrix in the liver, thus progressing to hepatic fibrosis. When treating hepatic fibrosis, LQAtta may exert its effects through mechanisms such as regulating the activation of hepatic stellate cells, inhibiting the release of inflammatory cytokines, and improving the redox state of the liver. Given the overlap in the pathological processes of NASH and hepatic fibrosis, we speculate that LQAtta can also improve the condition of NASH through these mechanisms or by further regulating the unique pathological links of NASH, such as lipid metabolism disorders. Based on previous research findings,<sup>18,19</sup> we will continue to focus on NASH, a growing global health challenge, and preliminarily explore the mechanism of action of LQAtta therein.

Metabolomics, an emerging field developed based on mass spectrometry technology, assesses the metabolic processes and functions of organisms by detecting and analyzing metabolomes.<sup>20</sup> Currently, the field of metabolomics, as highlighted in the work of Wu et al,<sup>21</sup> holds a pivotal role in elucidating the underlying material constituents and mechanisms of action associated with traditional Chinese medicines (TCMs). Consequently, this approach offers profound insights into the therapeutic efficacy and scientific rationale behind their use in treating a multitude of diseases. Network pharmacology<sup>22</sup> is a burgeoning discipline rooted in systems biology theory and biological system network analysis. It emphasizes the importance of identifying specificity signal nodes within complex biological networks, which can guide the design of multi-target drugs. These drugs are tailored to interact with multiple molecular targets simultaneously, offering a more holistic approach to treating diseases. The mechanism of action of TCM prescriptions has multi-target and multi-level characteristics, which are similar to the integrity, systematization, and comprehensiveness of network pharmacology. Therefore, network pharmacology is suitable for the pharmacological study of traditional Chinese medicine compounds.

This study aims to investigate the potential pathways of LQAtta in regulating NASH through metabolomics and mouse models and predict possible targets through network pharmacology. It is hoped that this research will provide new therapeutic approaches for the treatment of non-alcoholic fatty liver disease.

## Materials and Methods

### Experimental Animals

During this study, the animal experiment protocols received formal authorization from the Animal Protection and Experimental Animal Use and Management Committee of Jinling Clinical Medical College, Nanjing University of Chinese Medicine (Ethics Approval Number: DZISSDWLS240085), which ensured strict adherence to the guidelines established by the National Institutes of Health (NIH). The facility maintained for the animals was devoid of specific pathogens and controlled for both temperature and humidity, with a consistent 12-hour cycle of light and darkness. Mice, specifically male C57BL/6J weighing between 16 and 18 grams, were used. These mice had access to either standard or diet-specific food formulations, depending on the requirements of the study, and could drink from an unlimited supply of filtered water.

## Experimental Design

### Experimental Grouping

In the study, three experimental cohorts of mice, each consisting of eight individuals, were established through random allocation. The first cohort, referred to as the control group, received a standard dietary regimen. The second, identified as the model group, received a diet enriched with high levels of fat and cholesterol. The third group, designated as the LQAtta group, was subjected to a similar high-fat and high-cholesterol (HFHC) diet but was additionally treated with LQAtta.

### Establishment of Mouse Non-Alcoholic Steatohepatitis Model

For 20 weeks, a model for NASH was developed through the administration of a diet high in fat and cholesterol, consisting of 88% standard feed, 10% lard, and 2% cholesterol. Both the control group and the LQAtta group received an HFHC diet while having unlimited access to sterile water.

### LQAtta Treatment

At the 8-week mark of the induction phase, two mice were selected at random from each experimental group for model assessment. Following this, the mice subjected to an HFHC diet were further separated into two distinct subgroups: ① NASH group, and ② LQAtta group. The LQAtta group was fed with an HFHC diet supplemented with LQAtta until sacrifice at 16 weeks and 20 weeks.

## Drug Preparation

LQAtta<sup>18</sup> (Table 1) is *Bovis Calculus Artifactus*(0.1g), *Carthamus tinctorius* L. [Asteraceae](15g), *Trogopteroni faeces* (15g), *Phyllanthus emblica* L. [Phyllanthaceae](30g), *Swertia bimaculata* (Siebold & Zucc). Hook.f. and Thomson ex C. B. Clarke [Gentianaceae](15g), *Myristica fragrans* Houtt. [Myristicaceae](10g), *Astragalus mongholicus* Bunge [Fabaceae](25g), *Dolomiaea costus* (Falc). Kasana & A.K.Pandey [Asteraceae](10g), *Saxifraga stolonifera* Curtis [Saxifragaceae](15g), *Coriandrum sativum* L. [Apiaceae](10g), *Aquilaria sinensis* (Lour). Spreng. [Thymelaeaceae] (3g), *Punica granatum* L. [Lythraceae](20g), *Rhododendron anthopogonoides* Maxim. [Ericaceae](8g), *Malva verticillata* var. *verticillata* [Malvaceae](15g), and *Glycyrrhiza uralensis* Fisch. ex DC. [Fabaceae](10 g). The plant names have been verified using <http://www.plantsoftheworldonline.org>. The ratio is 0.02:3:3:6:3:2:5:2:3:2:0.6:4:1.6:3:2. *Bovis Calculus Artifactus*<sup>23</sup> is made from ox bile powder, cholic acid, hyodeoxycholic acid, taurine, bilirubin, cholesterol and trace elements. LQAtta granules were provided by Jiangsu Provincial Hospital of Integrated Traditional Chinese and

**Table 1** The Source and Composition of LQAtta

Chinese Name	English Name	Amount (g)	Scientific Names	Origin.	Batch No.
人工牛黄 Ren Gong Niu Huang	Artificial Cow-bezoar	0.1	<i>Bovis Calculus Artifactus</i> <sup>1</sup>	Bozhou Qiaojuntang Chinese Herbal Pieces Co., Ltd	2211011
红花 Hong Hua	Safflower	15	<i>Carthamus tinctorius</i> L. [Asteraceae]	Bozhou Qiaojuntang Chinese Herbal Pieces Co., Ltd	23051001
五灵脂 Wu Ling Zhi	/	15	<i>Trogopteroni faeces</i> <sup>2</sup>	Anhui Zhu's Pharmaceutical Chinese Herbal Pieces Co., Ltd	CJ - 446 - I - 240501
余甘子 Yu Gan Zi	Phyllanthi Fructus	30	<i>Phyllanthus emblica</i> L. [Phyllanthaceae]	Bozhou Qiaojuntang Chinese Herbal Pieces Co., Ltd	23050301
獐芽菜 Zhang Ya Cai	/	15	<i>Swertia bimaculata</i> (Siebold & Zucc). Hook.f. and Thomson ex C.B. Clarke [Gentianaceae]	Bozhou Qiaojuntang Chinese Herbal Pieces Co., Ltd	23050501
肉豆蔻 Rou Dou Kou	Nutmeg	10	<i>Myristica fragrans</i> Houtt. [Myristicaceae]	Anhui Zhu's Pharmaceutical Chinese Herbal Pieces Co., Ltd	CJ - 314 - I - 230201

(Continued)

Table 1 (Continued).

Chinese Name	English Name	Amount (g)	Scientific Names	Origin.	Batch No.
黄芪 Huang Qi	Milkvetch Root	25	<i>Astragalus mongholicus</i> Bunge [Fabaceae]	Anhui Zhu's Pharmaceutical Chinese Herbal Pieces Co., Ltd	CJ - 226-231001
木香 Mu Xiang	Aucklandiae Radix	10	<i>Dolomiaea costus</i> (Falc). Kasana & A.K.Pandey [Asteraceae]	Anhui Zhu's Pharmaceutical Chinese Herbal Pieces Co., Ltd	CJ - 036 - 236001
虎耳草 Hu Er Cao	Creeping Rockfoil	15	<i>Saxifraga stolonifera</i> Curtis [Saxifragaceae]	Bozhou Qiaojutang Chinese Herbal Pieces Co., Ltd	23050601
芫荽果 Yuan Sui Guo	Cilantro	10	<i>Coriandrum sativum</i> L. [Apiaceae]	Bozhou Qiaojutang Chinese Herbal Pieces Co., Ltd	23050701
沉香 Chen Xiang	Rosewood Heart Wood	3	<i>Aquilaria sinensis</i> (Lour). Spreng. [Thymelaeaceae]	Anhui Zhu's Pharmaceutical Chinese Herbal Pieces Co., Ltd	CJ - 596 - 240201
石榴子 Shi Liu Zi	Pomegranate	20	<i>Punica granatum</i> L. [Lythraceae]	Bozhou Qiaojutang Chinese Herbal Pieces Co., Ltd	23050301
烈香杜鹃 Lie Xiang Du Juan	Flos Rhododendri Anthopgoonoidi	8	<i>Rhododendron anthopogonoides</i> Maxim. [Ericaceae]	Bozhou Qiaojutang Chinese Herbal Pieces Co., Ltd	23050201
冬葵果 Dong Kui Guo	Fructus Malvae	15	<i>Malva verticillata</i> var. <i>verticillata</i> [Malvaceae]	Bozhou Qiaojutang Chinese Herbal Pieces Co., Ltd	23050801
甘草 Gan Cao	Liquorice Root	10	<i>Glycyrrhiza uralensis</i> Fisch. ex DC. [Fabaceae]	Anhui Zhu's Pharmaceutical Chinese Herbal Pieces Co., Ltd	CJ - 234 - 231201

Western Medicine. The names of the botanists who formally identified the plants and the references of the voucher specimens deposited in a public herbarium are provided in [Supplement Material 1](#).

### The Origin of Plant Materials

*Bovis Calculus Artifactus* was purchased from Bozhou Qiaojutang Chinese Herbal Pieces Co., Ltd (Batch No.: 2211011). *Carthamus tinctorius* L. was purchased from Bozhou Qiaojutang Chinese Herbal Pieces Co., Ltd (Batch No.: 23051001). *Trogopteroni faeces* was sourced from Anhui Zhu's Pharmaceutical Chinese Herbal Pieces Co., Ltd (Batch No.: CJ - 446 - 1 - 240501). *Phyllanthus emblica* L. was obtained from Bozhou Qiaojutang Chinese Herbal Pieces Co., Ltd (Batch No.: 23050301). *Swertia bimaculata* (Siebold & Zucc). Hook.f. and Thomson ex C.B. Clarke was bought from Bozhou Qiaojutang Chinese Herbal Pieces Co., Ltd (Batch No.: 23050501). *Myristica fragrans* Houtt. was bought from Anhui Zhu's Pharmaceutical Chinese Herbal Pieces Co., Ltd (Batch No.: CJ - 314 - 1 - 230201). *Astragalus mongholicus* Bunge was purchased from Anhui Zhu's Pharmaceutical Chinese Herbal Pieces Co., Ltd (Batch No.: CJ - 226 - 231001). *Dolomiaea costus* (Falc). Kasana & A.K.Pandey was sourced from Anhui Zhu's Pharmaceutical Chinese Herbal Pieces Co., Ltd (Batch No.: CJ - 036 - 236001). *Saxifraga stolonifera* Curtis was obtained from Bozhou Qiaojutang Chinese Herbal Pieces Co., Ltd (Batch No.: 23050601). *Coriandrum sativum* L. was bought from Bozhou Qiaojutang Chinese Herbal Pieces Co., Ltd (Batch No.: 23050701). *Aquilaria sinensis* (Lour). Spreng was sourced from Anhui Zhu's Pharmaceutical Chinese Herbal Pieces Co., Ltd (Batch No.: CJ - 596 - 240201). *Punica granatum* L. was purchased from Bozhou Qiaojutang Chinese Herbal Pieces Co., Ltd (Batch No.: 23050301). *Rhododendron anthopogonoides* Maxim was bought from Bozhou Qiaojutang Chinese Herbal Pieces Co., Ltd (Batch No.: 23050201). *Malva verticillata* var. *verticillata* was obtained from Bozhou Qiaojutang Chinese Herbal Pieces Co., Ltd (Batch No.: 23050801). *Glycyrrhiza uralensis* Fisch. ex DC. was sourced from Anhui Zhu's Pharmaceutical Chinese Herbal Pieces Co., Ltd (Batch No.: CJ - 234 - 231201).

In the prescription, *Myristica fragrans*, *Coriandrum sativum*, *Dolomiaea costus*, *Aquilaria malaccensis*, and *Rhododendron anthopogonoides* were extracted with ten times their volume of water using steam distillation for five hours to collect volatile oil. The aqueous extract and herbal residue were stored separately. Volatile oil- $\beta$ -cyclodextrin inclusion complexes were prepared by first dissolving  $\beta$ -cyclodextrin in water heated to 60°C in a ratio of volatile oil:  $\beta$ -

cyclodextrin: water (1:10:100), then adding the volatile oil with stirring for four hours. After cooling, the mixture was refrigerated overnight, filtered, and the precipitate was dried at 40°C and crushed for storage. Additionally, *Carthamus tinctorius*, *Trogopterori faeces*, *Phyllanthus emblica*, *Astragalus mongholicus* Bunge, *Swertia bimaculata*, *Saxifraga stolonifera*, *Malva verticillata*, *Punica granatum*, and *Glycyrrhiza uralensis*, along with the herbal residue from the volatile oil extraction of *Myristica fragrans* et al, were decocted three times with ten times their volume of water for one hour each. The decoctions were filtered, and the filtrates were combined with the previous aqueous extract. The combined filtrate was concentrated under reduced pressure to form an extract with a relative density of 1.05 to 1.10 at 60°C. After cooling and centrifugation, the supernatant was further concentrated into an extract with a relative density of 1.25 to 1.30 at 60°C. The concentrated extract was then dried under reduced pressure, crushed, and stored as dry extract powder. Finally, *Bovis Calculus Artificatus*, the dry extract powder, volatile oil- $\beta$ -cyclodextrin inclusion complexes, dextrin, and stevioside were mixed uniformly, granulated, and packaged to obtain the final product.

In previous experiments,<sup>18,19</sup> based on the body surface area and human/rat dose conversion, different doses of LQAtta have been used (11 g/kg, 5.5 g/kg, 2.75 g/kg), and 11 g/kg was found to have good efficacy. Therefore, in this study, a dose of 11 g/kg LQAtta was selected.

## Reagents and Instruments

LC-MS grade methanol (MeOH) was purchased from Fisher Scientific (Loughborough, UK). 2-Amino-3-(2-chloro-phenyl)-propionic acid was obtained from Aladdin (Shanghai, China). Ultrapure water was generated using a Milli-Q system (Millipore, Bedford, USA). Acetonitrile (ACN) was purchased from Fisher Scientific (Loughborough, UK). Formic acid was obtained from TCI (Shanghai, China). Ammonium formate was obtained from Sigma-Aldrich (Shanghai, China). Ultrapure water was generated using a Milli-Q system (Millipore, Bedford, USA).

High-speed freezing centrifuge was obtained from Hunan Xiangyi Experiment Equipment Co., Ltd. (Hunan, China). The vortex mixer was obtained from Haimen Kylin-bell Lab Instruments Co., Ltd. (Haimen, China). The centrifugal vacuum evaporator was from Eppendorf China Ltd. (Shanghai, China). Ultrasonic cleaner was obtained from Kunshan Shumei Experiment Equipment Co., Ltd. (Kunshan, China). The tissue grinder was obtained from Zhejiang Meibi Experiment Equipment Co., Ltd. (Zhejiang, China). Microporous membrane filters (0.22  $\mu$ m) were purchased from Tianjin Jinteng Experiment Equipment Co., Ltd. (Tianjin, China).

## Sample Preparation and On-Machine Detection

### Drug Sample Preparation

Accurately weigh an appropriate amount of sample into a 2 mL centrifuge tube, add 600  $\mu$ L MeOH (Containing 2-Amino-3-(2-chloro-phenyl)-propionic acid(4 ppm), vortex for 30s; Add steel balls, placed in a tissue grinder for 60s at 55 Hz; Room temperature ultrasound for 15 min; Centrifuge for 10 min at 12,000 rpm and 4°C, filter the supernatant by 0.22  $\mu$ m membrane, and transfer into the detection bottle for LC-MS detection.<sup>24</sup>

### Serum Sample Preparation

Thaw the experimental sample at 4°C, vortex the sample for 1 min after thawing, and mix evenly; Accurately transfer an appropriate amount of sample into a 2 mL centrifuge tube; Add 400  $\mu$ L methanol and vortex for 1 min; Centrifuge for 10 min at 12,000 rpm and 4 °C, take all the supernatant transfer it to a new 2 mL centrifuge tube, concentrate, and dry it; Add 150  $\mu$ L of 2-chloro-l-phenylalanine (4 ppm) solution prepared with 80% methanol-water to redissolve the sample, filter the supernatant by 0.22  $\mu$ m membrane and transfer it into the detection bottle for LC-MS detection.<sup>25</sup>

### On-Machine Detection

#### Liquid Chromatography Conditions

The LC analysis was performed on a Vanquish UHPLC System (Thermo Fisher Scientific, USA). Chromatography was carried out with an ACQUITY UPLC<sup>®</sup> HSS T3 (2.1 $\times$ 100 mm, 1.8  $\mu$ m) (Waters, Milford, MA, USA). The column was maintained at 40 °C. The flow rate and injection volume were set at 0.3 mL/min and 2  $\mu$ L, respectively. For LC-ESI (+)-MS analysis, the mobile phases consisted of (B2) 0.1% formic acid in acetonitrile (v/v) and (A2) 0.1% formic acid in

water (v/v). Separation was conducted under the following gradient: 0~1 min, 8% B2; 1~8 min, 8%~98% B2; 8~10 min, 98% B2; 10~10.1 min, 98%~8% B2; 10.1~12 min, 8% B2. For LC-ESI (-)-MS analysis, the analytes were carried out with (B3) acetonitrile and (A3) ammonium formate (5 mM). Separation was conducted under the following gradient: 0~1 min, 8% B3; 1~8 min, 8%~98% B3; 8~10 min, 98% B3; 10~10.1 min, 98%~8% B3; 10.1~12 min, 8% B3.<sup>26</sup>

### Mass Spectrum Conditions

Mass spectrometric detection of metabolites was performed on Q Exactive Focus (Thermo Fisher Scientific, USA) with ESI ion source. Simultaneous MS1 and MS/MS (Full MS-ddMS2 mode, data-dependent MS/MS) acquisition was used. The parameters were as follows: sheath gas pressure, 40 arb; aux gas flow, 10 arb; spray voltage, 3.50 kV and -2.50 kV for ESI(+) and ESI(-), respectively; capillary temperature, 325 °C; MS1 range, m/z 100–1000; MS1 resolving power, 70000 FWHM; number of data dependant scans per cycle, 3; MS/MS resolving power, 17500 FWHM; normalized collision energy, 30 eV; dynamic exclusion time, automatic.<sup>27</sup>

## Network Pharmacological Analysis

### Acquisition of Chemical Components and Disease Targets

The chemical components of “Bovis Calculus Artifactual”, “Carthamus tinctorius”, “Phyllanthus emblica”, and “Saxifraga stolonifer” were retrieved from the TCSMP database at <https://old.tcmsp-e.com/>. Active components were selected based on the criteria of “OB  $\geq$  30% and DL  $\geq$  0.18”. The targets of these active components were searched for, and the corresponding Gene symbols for the protein targets were identified through the UniProt database at <https://www.uniprot.org/>. Additionally, the active components and their targets of “Swertia bimaculata” and “Trogopteroni faeces” were searched using the BATMAN database at <http://bionet.ncpsb.org.cn/batman-tcm/>, with the criteria of “Score cutoff  $>$  20 and Adjusted P-value  $<$  0.05”. The identified targets were then standardized using the UniProt database. With “NASH” as the disease term, keywords were searched in the GeneCards database at <https://www.genecards.org/> and the OMIM database at <https://omim.org/mimmatch/>. Duplicate entries were removed after merging. The Venny 2.1 platform was utilized to draw a Venn diagram for screening common targets between chemical components and the disease.

### Construction of Protein-Protein Interaction (PPI) Network and Acquisition of Core Targets

The common targets were imported into the String database at <https://string-db.org/>. The mode was set to “multiple proteins”, and the organism was selected as Homo sapiens. The minimum required interaction score was set to 0.7 to remove single proteins without interactions. The downloaded TSV file was imported into Cytoscape 3.8.2 software, and the CytoNCA plugin was used to calculate the Degree of Centrality (DC). The top 20 targets with the highest DC values were selected as core targets. Simultaneously, the PPI network diagram was drawn using Cytoscape software.

### GO Enrichment Analysis and KEGG Pathway Analysis

The 20 core targets were individually imported into the DAVID database at <https://david.ncifcrf.gov/> for GO (Gene Ontology) enrichment analysis and KEGG (Kyoto Encyclopedia of Genes and Genomes) pathway analysis, with Homo sapiens selected as the species. Visualizations were conducted using the Weishengxin platform at <http://www.bioinformatics.com.cn/>.

### Construction of the “Component-Core Target-Pathway” Diagram

The Cytoscape software was used to construct and analyze the component-target-pathway diagram. Nodes represented chemical components, core targets, and pathways, while edges represented the interaction relationships between nodes.

## Assays for Serum and Liver Biochemical Markers

After the LQAtta treatment, mice were anesthetized with 3% pentobarbital, their whiskers were trimmed, and the eyeballs were removed. Blood samples were drawn into tubes that included a clotting agent, and then subjected to centrifugation at 3000 rpm for 15 minutes at ambient temperature. Following this, the separated serum layer was meticulously isolated and subsequently preserved at a temperature of -80°C, ensuring its availability for upcoming

analytical procedures. Following blood collection, mice underwent euthanasia through cervical dislocation. The liver was then visually inspected for any gross morphological changes before being excised and weighed. For histological evaluation, a liver lobe segment was fixed in 4% paraformaldehyde solution overnight, followed by preparation for embedding and subsequent sectioning. The residual liver tissue was immediately transferred to cryotubes and subsequently immersed in liquid nitrogen, ensuring preservation for forthcoming experimental procedures.

The assessment of liver functionality and lipid profiles within the bloodstream utilized a state-of-the-art fully automated biochemical analyzer. The assessments done in this analysis involved some parameters that are relevant to liver function such as alanine aminotransferase (ALT) and aspartate aminotransferase (AST). Moreover, the assessment of lipid profile focused on the measurement of Total Cholesterol (CHO).

## Histopathological Examination of the Liver

Histopathological evaluation of liver tissue: The histological examination of different structures and in particular the presence of lipids in the liver sections of mice was done using both the HE staining procedure and Oil Red O staining methods. Also, the degree of fibrosis was assessed from the Sirius Red staining of these sections.

## Immunohistochemical Staining

Evaluation of immune cell infiltration: To evaluate the extent of infiltration by macrophages and CD4 and CD8 T cells in mouse liver tissue, sections were subjected to immunohistochemical analysis using antibodies specific for F4/80, CD4, and CD8 markers. In addition, immunohistochemistry of p-NF- $\kappa$ B p65 and NF- $\kappa$ B p65 was also performed. This method allowed for a detailed assessment of immune cell presence within the hepatic environment.

## Quantification of mRNA Expression

Detailed quantitative evaluations were conducted to accurately measure the levels of specific proinflammatory cytokines, which include IL-1 $\beta$ , IL-6, and TNF- $\alpha$ , present in samples of liver tissue.

Total RNA was extracted from liver samples using TRIzol reagent (GlpBio Technology, GK20008-100). Reverse transcription was then performed using HiScript<sup>®</sup> II Q RT SuperMix (Vazyme Biotech, R223-01) according to the manufacturer's instructions. The PCR amplification products were quantified using a real-time PCR system (LightCycler480 Instrument II) in conjunction with SYBR Green reagent (Vazyme Biotech, Q711-02). The mRNA expression levels of target genes were normalized to that of  $\beta$ -actin using the comparative CT ( $2^{-\Delta\Delta C_t}$ ) method. The primer sequences for mice are listed in Table 2.

## Western Blotting

Liver tissue extracts were lysed using Radioimmunoprecipitation (RIPA) buffer containing a protease inhibitor cocktail (GlpBio Technology, GK10014) and a phosphatase inhibitor cocktail (GlpBio Technology, GK10012). For Western blot analysis, equal amounts of protein were subjected to Sodium Dodecyl Sulfate-Polyacrylamide Gel Electrophoresis (SDS-PAGE) and subsequently electrotransferred onto PVDF membranes (Millipore). The membranes were incubated in 5% skimmed milk or 3% bovine serum albumin before being blotted with specific primary antibodies. Following incubation with horseradish peroxidase (HRP)-conjugated secondary antibodies, the membranes were detected using a chemiluminescent Western blot detection system (Bio-Rad Laboratories, CA, USA). Density measurements were performed using ImageJ software (Fujifilm, Tokyo, Japan).

**Table 2** Synthetic Oligonucleotide Primers Employed for RT-qPCR Evaluations

Gene	Forward Primer	Reverse Primer
NF- $\kappa$ B	ATGGCAGACGATGATCCCTAC	TGTTGACAGTGGTATTTCTGGTG
IL-1 $\beta$	TGGACCTTCCAGGATGAGGACA	GTTTCATCTCGGAGCCTGTAGTG
TNF- $\alpha$	CAGGCGGTGCCTATGTCTC	CGATCACCCCGAAGTTCAGTAG
IL-6	TAGTCCTTCCACCCCAATTTCC	TTGGTCCTTAGCCACTCCTTC
GAPDH	AGGTCGGTGTGAACGGATTTG	TGTAGACCATGTAGTTGAGGTCA

Detection of NF- $\kappa$ B Pathway Indicators: The technique of Western blotting was utilized to assess the levels of p-NF- $\kappa$ B p65 and NF- $\kappa$ B p65 in liver tissues.

## Results

### Analysis of LQAtta Granule Composition and Blood Entry Composition

After gavage administration of LQAtta to HFHC mice, their serum was collected as drug-containing serum, while the serum of HFHC mice without drug administration served as control serum. Both drug-containing serum and control serum underwent non-targeted metabolome sequencing (Figure 1B). The metabolites obtained from both groups were intersected to identify common metabolites (Figure 1D). Subsequently, the common metabolites in the drug-containing serum group were excluded, leaving 260 unique metabolites in the drug-containing serum group. Further comparison of these 260 unique metabolites in the drug-containing serum group with the 1518 secondary metabolites of the LQAtta granule identified a total of 106 blood-entry components of LQAtta (Table 3).

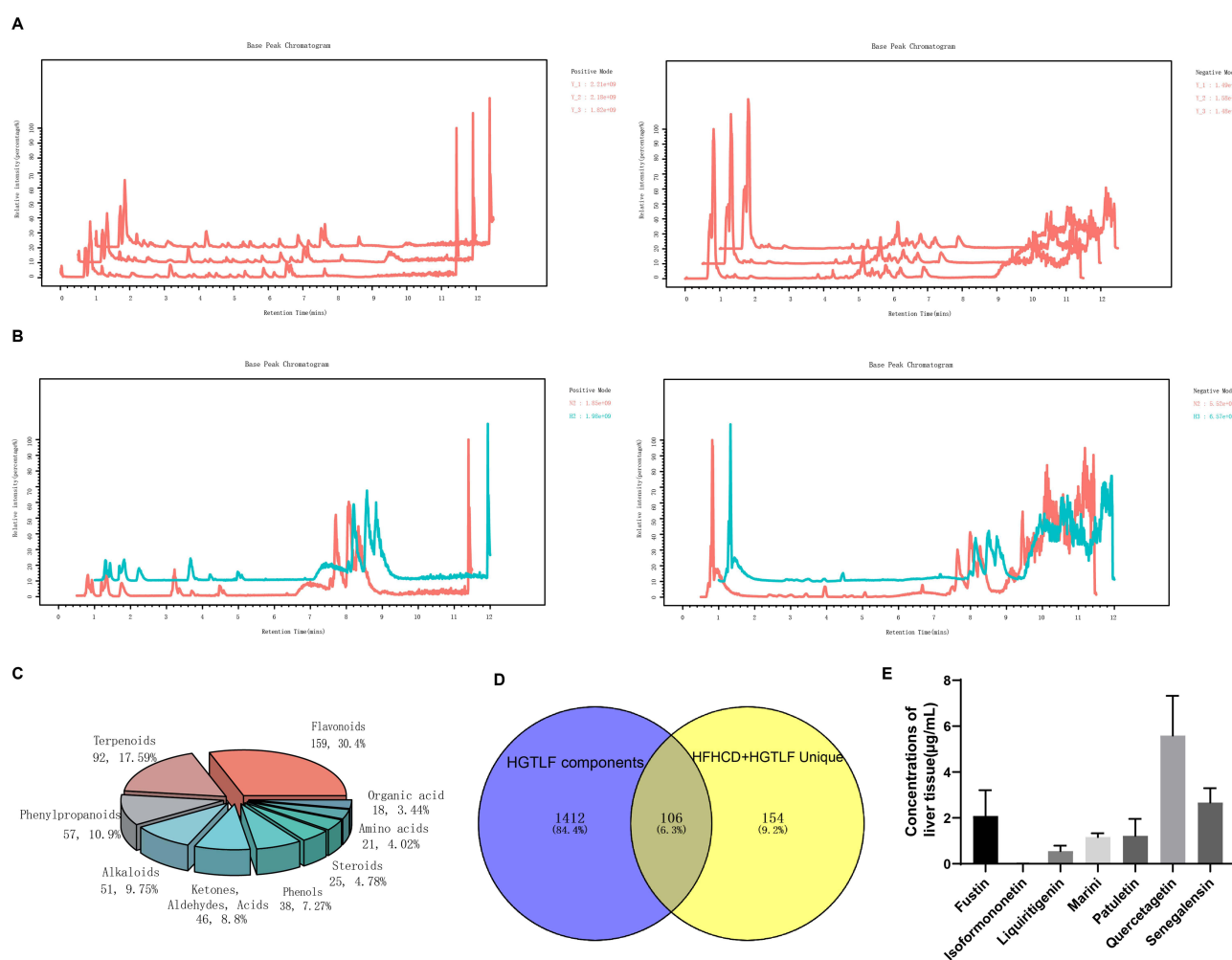


**Figure 1** Analysis of LQAtta granule composition and blood entry composition. UPLC-MS/MS was utilized for non-targeted metabolome sequencing of the components of the LQAtta granule (**A** and **C**), the serum of HFHC mice without drug administration (control serum), and the serum of HFHC mice after gavage administration of LQAtta (drug-containing serum). (**A**) Positive and negative ion base peak chromatograms of LQAtta granule. (**B**) Positive and negative ion base peak chromatograms of typical samples from control serum and drug-containing serum. (**C**) A total of 1518 secondary metabolites were identified in the LQAtta granule. Statistical analysis was conducted on the categories of these metabolites and presented in a pie chart, with flavonoids being the most abundant, totaling 159 and accounting for 30.4% of all metabolites. (**D**) Unique substances were screened from both the control serum and drug-containing serum, resulting in 260 unique substances in the drug-containing serum. These unique substances were then compared with the results of individual identification of LQAtta granules, and a total of 106 blood-entry components of LQAtta were identified among the unique substances in the drug-containing serum (Table 3). In this figure, HGTLF is LQAtta. (**E**) HPLC technology was employed to detect the concentrations of all blood-entry flavonoids (Fustin, Isoformononetin, Liquiritigenin, Marini, Patuletin, Quercetagenin, Senegalensin) in the liver tissue of mice. N=5.

**Table 3** 106 Components Entering the Blood

NO.	Name	mz	rt	Formula	Precursor_type
1	(3s)-3,6-diaminohexanoate	129.1029	574.9	C6H14N2O2	[M-H2O+H]+
2	(s)-ureidoglycolic acid	173.1288	83.8	C3H6N2O4	[M+K]+
3	l-aminocyclopropane-1-carboxylate	102.0554	16.2	C4H7NO2	[M+H]+
4	l-methylhistamine	126.1028	44.4	C6H11N3	[M+H]+
5	1,2-dibutylin	293.0484	53.3	C11H20O5	[M+HCO3]-
6	1,4-dihydroxynaphthalene	178.1086	625.3	C10H8O2	[M+NH4]+
7	18-hydroxyoleic acid	279.2323	626.5	C18H34O3	[M-H2O-H]-
8	2-cyclohexen-1-one	114.0913	200.7	C6H8O	[M+NH4]+
9	2-hexyldecanoic acid	511.4725	604.1	C16H32O2	[2M-H]-
10	2-hydroxyphenazine	195.0491	333	C12H8N2O	[M-H]-
11	2-methyl-5-(8-pentadecenyl)-1,3-benzenediol	355.2625	392.1	C22H36O2	[M+Na]+
12	2-oxo-5-methylthiopentanoic acid	207.0658	221.5	C6H10O3S	[M+HCOO]-
13	2-phenylethyl acetate	203.1837	55.8	C10H12O2	[M+K]+
14	2,4-dihydroxy-7-methoxy-2h-1,4-benzoxazin-3(4h)-one	250.1437	200.9	C9H9NO5	[M+K]+
15	2,4-pentanedione	145.0862	689	C5H8O2	[M+HCOO]-
16	2,4,6-trinitrotoluene	228.0218	52.5	C7H5N3O6	[M+H]+
17	2,6-dimethylpyrazine	109.0765	582.9	C6H8N2	[M+H]+
18	3-(indol-3-yl)pyruvate	159.0665	676.7	C11H8NO3-	[M-CO2+H]+
19	3-buten-2-one	141.0904	180.8	C4H6O	[2M+H]+
20	3-hexanone	123.0792	629.2	C6H12O	[M+Na]+
21	3-methyl-2-butenal	102.0918	55.8	C5H8O	[M+NH4]+
22	4-butyl-gamma-butyrolactone	126.0664	73.1	C8H14O2	[M-OH+H]+
23	4-hydroxycinnamic acid	163.0397	186.4	C9H8O3	[M-H]-
24	5-amino-4-imidazole carboxylate	188.0203	52.1	C4H5N3O2	[M+HCO3]-
25	Acibenzolar	152.995	27.7	C7H4N2OS2	[M-CO2+H]+
26	Aklavin	614.2201	303.7	C30H35NO10	[M+HCOO]-
27	Aloin	835.2482	38.6	C21H22O9	[2M-H]-
28	Alpha-curcumene	186.1551	638.5	C15H22	[M-NH3+H]+
29	Alpha-ketoisovaleric acid	115.0391	689	C5H8O3	[M-H]-
30	Anisole	109.0762	606.3	C7H8O	[M+H]+
31	Ascorbigen	611.189	537.8	C15H15NO6	[2M+H]+
32	Camptothecin	695.2209	398.4	C20H16N2O4	[2M-H]-
33	Capsiconiate	316.2121	222.3	C20H28O4	[M-NH3+H]+
34	Chrysophanol	253.0511	308.3	C15H10O4	[M-H]-
35	Cis-zeatin	202.1086	587.8	C10H13N5O	[M-H2O+H]+
36	Cyclo(leu-phe)	321.1477	279	C15H20N2O2	[M+HCO3]-
37	D-glucuronic acid	177.0394	70.2	C6H10O7	[M-H2O+H]+
38	Dehydroabiatic acid	299.2017	519.7	C20H28O2	[M-H]-
39	Dehydroascorbic acid	173.0085	45.1	C6H6O6	[M-H]-
40	Delta8,14-sterol	394.3541	573.3	C29H46O	[M-OH+H]+
41	Demethylphyloquinone	481.3315	656.7	C30H44O2	[M+HCOO]-
42	Deoxycholic acid	437.2908	340.2	C24H40O4	[M+HCOO]-
43	Dihydroxyacetone phosphate	214.9957	45.6	C3H7O6P	[M+HCOO]-
44	Dihydrozeatin	204.1215	72.6	C10H15N5O	[M-H2O+H]+
45	Dimethylurea	111.0749	617.8	C3H8N2O	[M+Na]+
46	Dopamine quinone	169.0948	46	C8H9NO2	[M+NH4]+
47	Dtxsid60975124	533.1594	420	C14H29N6O11P	[M+HCOO]-
48	Epinephrine	184.0943	51	C9H13NO3	[M+H]+
49	Epsilon-caprolactone	159.0655	689	C6H10O2	[M+HCOO]-
50	Fa 20_1	328.2851	536.2	C20H38O2	[M+NH4]+
51	Fa 20_5;o2	352.3204	559.2	C20H30O4	[M+NH4]+

(Continued)

Table 3 (Continued).

NO.	Name	mz	rt	Formula	Precursor_type
52	Fructose	161.046	143.2	C6H12O6	[M-H2O-H]-
53	Fumaric acid	115.0386	73	C4H4O4	[M-H]-
54	Fusarindin	257.1765	287.5	C14H10O5	[M-H]-
55	Fustin	287.06	286.6	C15H12O6	[M-H]-
56	G-418	497.3511	484	C20H40N4O10	[M+H]+
57	Glutaric acid	155.0454	192.7	C5H8O4	[M+Na]+
58	Glycerol tributanoate	347.1715	516.1	C15H26O6	[M+HCOO]-
59	Glycerophosphocholine	280.0902	49.9	C8H20NO6P	[M+Na]+
60	Glycyrrhetol	913.7286	317.6	C30H48O3	[2M+H]+
61	Harmaline	259.1085	236.2	C13H14N2O	[M+HCOO]-
62	Hop ether	153.1275	30.3	C10H16O	[M+H]+
63	Indole-3-acetylglutamic acid	607.211	414.6	C15H16N2O5	[2M-H]-
64	Isoeugenol	225.0764	120.6	C10H12O2	[M+HCO3]-
65	Isoformononetin	249.0576	72	C16H12O4	[M-H2O-H]-
66	Isoliquiritigenin	255.069	662	C15H12O4	[M-H]-
67	Isonicotinic acid	124.0402	43.4	C6H5NO2	[M+H]+
68	Isopimpinellin	227.0383	292.9	C13H10O5	[M-H2O-H]-
69	Isoscopoletin	191.0341	84.5	C10H8O4	[M-H]-
70	L-isoleucine	132.1018	64.9	C6H13NO2	[M+H]+
71	Linamarin	248.113	84.8	C10H17NO6	[M+H]+
72	Liquiritigenin	255.0692	447.8	C15H12O4	[M-H]-
73	M-toluic acid	158.9886	324.5	C8H8O2	[M+Na]+
74	Marini	405.173	587.8	C25H28O6	[M-H2O-H]-
75	Marmesin	307.0841	54.7	C14H14O4	[M+HCO3]-
76	Methyl nonanoate	156.1496	662.7	C10H20O2	[M-OH+H]+
77	Methyleugenol	217.1983	94.9	C11H14O2	[M+K]+
78	Myo-inositol	179.0549	52.6	C6H12O6	[M-H]-
79	N-(p-hydroxyphenyl)ethyl p-hydroxycinnamide	265.0832	84.5	C17H17NO3	[M-NH3-H]-
80	N-acetyl-d-glucosamine	178.1087	606.6	C8H15NO6	[M-CO2+H]+
81	N-acetyl-l-phenylalanine	206.0816	168.6	C11H13NO3	[M-H]-
82	N4-acetylaminobutanal	113.071	662.2	C6H11NO2	[M-NH3+H]+
83	Naloxone	328.1387	98.4	C19H21NO4	[M+H]+
84	Norathyriol	259.0284	226.7	C13H8O6	[M-H]-
85	Ouabain	585.3593	211.8	C29H44O12	[M+H]+
86	P-cresol	126.0916	56.8	C7H8O	[M+NH4]+
87	Paraxanthine	161.046	222.6	C7H8N4O2	[M-H2O-H]-
88	Patuletin	393.0445	308.3	C16H12O8	[M+HCO3]-
89	Pc_38_4	854.5869	570.4	C46H84NO8P	[M+HCOO]-
90	Pc(o-16_0_20_3(8z,11z,14z))	830.5618	29.7	C44H84NO7P	[M+HCO3]-
91	Phenylacetyl glycine	192.0656	149	C10H11NO3	[M-H]-
92	Picrocrocin	329.1612	268.5	C16H26O7	[M-H]-
93	Pinostilbene	303.0918	566.9	C15H14O3	[M+HCO3]-
94	Pipecolic acid	130.0497	73.1	C6H11NO2	[M+H]+
95	Pseudouridine	243.0622	4	C9H12N2O6	[M-H]-
96	Pyrazin-2-carboxylic acid	142.0529	43.4	C5H4N2O2	[M+NH4]+
97	Pyridoxamine	191.1043	47.4	C8H12N2O2	[M+Na]+
98	Quercetagetin	379.0344	584.2	C15H10O8	[M+HCO3]-
99	Resveratrol	227.2015	550.8	C14H12O3	[M-H]-
100	Ricinine	327.1111	498.2	C8H8N2O2	[2M-H]-
101	Salicylic acid	137.0344	73	C7H6O3	[M-H]-

(Continued)

**Table 3** (Continued).

NO.	Name	mz	rt	Formula	Precursor_type
102	Schembl498748	159.9927	8.3	C <sub>6</sub> H <sub>5</sub> ClO <sub>4</sub>	[M-OH+H] <sup>+</sup>
103	Senegalensin	453.2853	308.5	C <sub>25</sub> H <sub>28</sub> O <sub>5</sub>	[M+HCOO] <sup>-</sup>
104	Sorbose	241.0565	390.1	C <sub>6</sub> H <sub>12</sub> O <sub>6</sub>	[M+HCO <sub>3</sub> ] <sup>-</sup>
105	Tetracosanoic acid	367.3576	605.4	C <sub>24</sub> H <sub>48</sub> O <sub>2</sub>	[M-H] <sup>-</sup>
106	Theobromine	179.0555	689	C <sub>7</sub> H <sub>8</sub> N <sub>4</sub> O <sub>2</sub>	[M-H] <sup>-</sup>

## Network Pharmacology Analysis

Based on the TCMSP and BATMAN databases, 388 chemical component targets were obtained; after searching and deduplication from the Genecards and OMIM databases, a total of 4011 potential targets were identified. By intersecting the chemical component targets with the disease targets, 160 common targets were obtained, indicating that these targets may be the potential therapeutic targets of LQAtta (Figure 2A). Subsequently, we constructed a Protein-Protein Interaction (PPI) network to depict the intricate relationships among different targets. We identified 20 core target signals (Figure 2B). GO enrichment analysis determined the biological processes associated with the hepatoprotective effects of LQAtta, mainly involving responses to oxidative stress, apoptosis, and inflammation (Figure 2C). KEGG enrichment analysis suggested that LQAtta may alleviate NASH by regulating pathways such as the Toll-like receptor signaling pathway, the NF- $\kappa$ B signaling pathway, and inflammation-related pathways (Figure 2D). Finally, the Cytoscape software was utilized to create a component-target-pathway network diagram (Figure 2E).

## Improvement of Body Weight and Fat Accumulation in HFHC-Induced NASH Mice by LQAtta

To evaluate the impact of LQAtta on NASH, HFHC-induced NASH mice were employed in this study. C57 BL/6J mice were fed with an HFHC diet for 8 weeks. Subsequently, the treatment group received HFHC+LQAtta for 8 and 12 weeks, while the NASH group continued to be fed with HFHC for 8 and 12 weeks consecutively (Figure 3A). The results revealed differences in the weight gain curves among the three groups. From the 16th to the 20th week post-treatment, HFHC-fed NASH mice exhibited significantly increased body weights compared to those in the normal diet group. Furthermore, the LQAtta group exhibited a marked reduction in body weight from the 16th to the 20th week of treatment, compared to the HFHC group (Figure 3B). Additionally, gross morphological examination of the liver revealed that the livers of NASH group mice were significantly enlarged, yellowish in color, with a slightly tough texture, blunt edges, and a greasy appearance, accompanied by a significant increase in liver weight. In contrast, the livers of mice in the HFHC +LQAtta group were smaller in size, with improved coloration and softer texture, compared to those in the NASH group, and the liver weight was reduced (Figure 3C and D).

## LQAtta Alleviates Hepatic Steatosis and Improves Lipid Metabolism in NASH Mice

To evaluate the therapeutic efficacy of LQAtta against HFHC-induced liver injury, serum ALT and AST levels were measured. The results demonstrated a significant reduction in serum ALT levels following LQAtta administration, whereas serum AST levels showed no significant difference from the NASH group at week 20 (Figure 4A). To assess the impact of LQAtta on lipid metabolism in NASH mice, serum lipid levels were examined. HFHC feeding notably elevated serum CHO levels, which were subsequently reduced by LQAtta treatment. Notably, TG levels did not follow the conventional trend of elevation in the NASH group and subsequent reduction in the treated group as reported in previous literature (Figure 4A). To further evaluate the effects of LQAtta on hepatic steatosis and lipid accumulation in NASH mice, H&E staining was employed to assess steatosis, Oil Red O staining was used to quantify hepatic lipid droplet accumulation, and Sirius Red staining was applied to evaluate liver collagen fiber content. From weeks 16 to 20 post-treatment, H&E staining revealed that LQAtta progressively mitigated liver injury and steatosis in NASH mice (Figure 4B). NAS scores<sup>28</sup> of liver H&E images are shown in Table 4. Oil Red O staining indicated that LQAtta

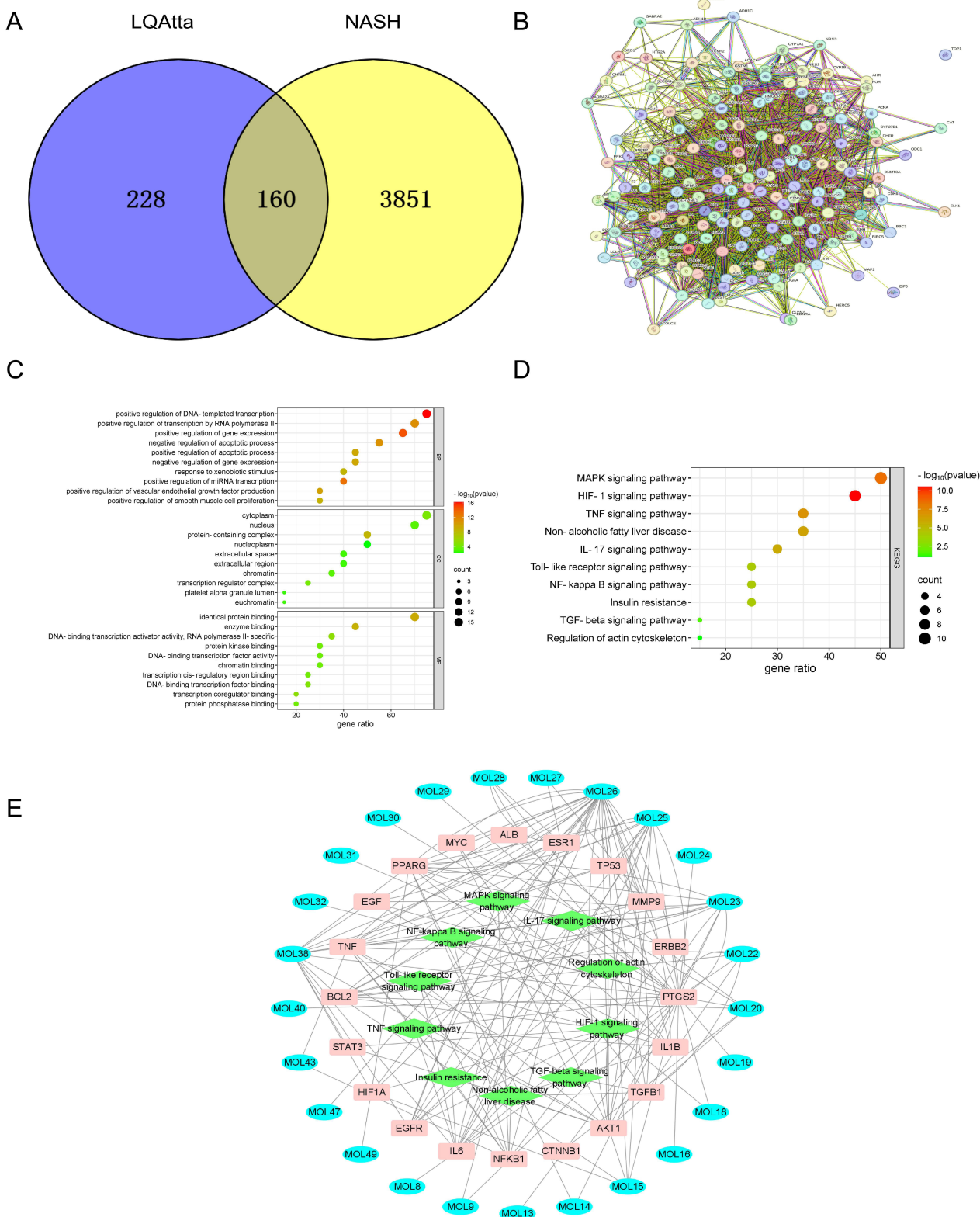


**Figure 2** Identification of Core Targets, GO Enrichment Analysis, and KEGG Pathway Analysis for LQAtta's Anti-NASH Effects. **(A)** Venn Diagram of LQAtta Component-Related and NASH-Related Targets. **(B)** PPI Construction Diagram. **(C)** GO Enrichment Analysis of LQAtta's Anti-NASH Targets. **(D)** Bubble Plot of KEGG Enrichment Analysis of LQAtta's Anti-NASH Targets. **(E)** Component-Core Target-Pathway Diagram.

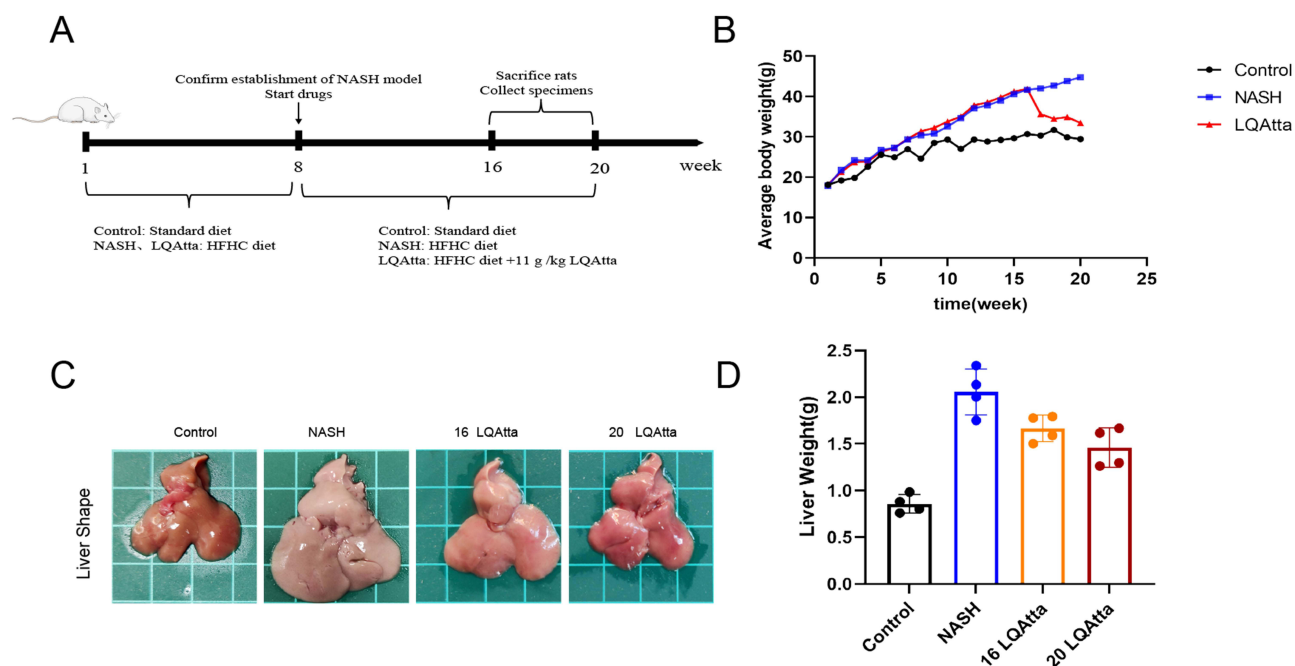


**Figure 3** Improvement of Body Weight and Fat Accumulation in HFHC-Induced NASH Mice by LQAtta. (A). Experimental flowchart outlining the study design. (B). Changes in body weight across different groups. (C). Representative images of mouse livers, illustrating the effects of treatment. (D). Quantitative analysis of liver weight in representative mice.  $n = 4$ .

treatment ameliorated hepatic lipid accumulation (Figure 4C). Sirius Red staining demonstrated that liver fibrosis was significantly reduced in the LQAtta-treated group compared to the model group (Figure 4D). Collectively, these findings suggest that LQAtta administration alleviates hepatic steatosis and improves lipid metabolism in NASH mice.

### Potential Regulation of NASH by LQAtta via the NF- $\kappa$ B Pathway

To evaluate the protein-level modulation of NASH by LQAtta, validation was performed through Western blotting (Figure 5A and B). The results demonstrated that the p-NF- $\kappa$ B p65 protein levels in the livers of mice in the NASH group were significantly higher than those in the control group ( $P < 0.05$ ). Conversely, the expression levels of p-NF- $\kappa$ B p65 protein in the LQAtta group were notably lower than those in the NASH group. To further assess the mRNA-level regulation of NASH by LQAtta, RT-qPCR analysis revealed (Figure 5C) that compared to the control group, the mRNA expression levels of inflammatory factors (TNF- $\alpha$ , IL-1 $\beta$ , IL-6) and NF- $\kappa$ B in the livers of mice in the model group were significantly upregulated. After 20 weeks of intervention with LQAtta, the mRNA expression of TNF- $\alpha$ , IL-1 $\beta$ , IL-6, and NF- $\kappa$ B were all downregulated. In summary, LQAtta may regulate NASH through the NF- $\kappa$ B pathway.

### Improvement of Immunohistochemical Levels in HFHC-Induced NASH Mice by LQAtta

To evaluate the infiltration of macrophages and CD4<sup>+</sup> and CD8<sup>+</sup> T cells in mouse liver tissues, immunohistochemical analysis was conducted on tissue sections using specific antibodies against F4/80, CD4, and CD8 markers. The F4/80 immunohistochemical staining (Figure 6A) showed that compared to control mice, there was a significant increase in macrophage infiltration in the HFHC diet-induced model group, while intervention with LQAtta reduced macrophage infiltration in mice fed the HFHC diet. Figures 6B and (Figure 6C) present the immunohistochemical staining for CD4 and CD8, respectively, revealing that compared to control mice, there was a marked increase in immune cell infiltration in the NASH group, which was mitigated by LQAtta intervention. Nuclear immunohistochemical staining (Figure 6D) demonstrated that the p-NF- $\kappa$ B p65 protein level in the NASH group was significantly higher than that in the control

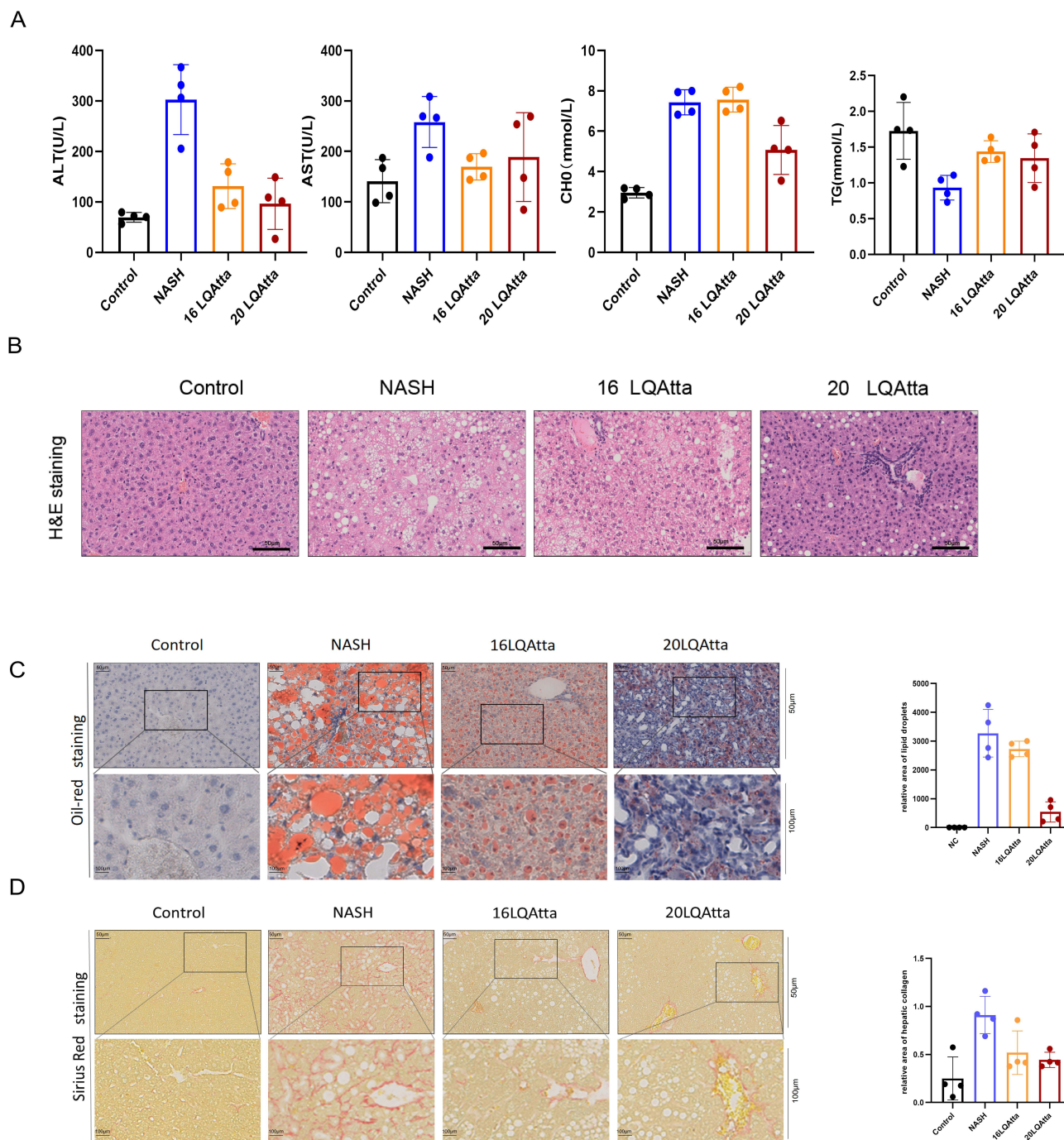


**Figure 4** LQAtta alleviates hepatic steatosis and improves lipid metabolism in NASH mice. **(A)**. Serum levels of ALT, AST, CHO, and TG in mice. **(B)**. Representative images of liver sections stained with H&E. **(C)**. Representative images and quantitative analysis of liver sections stained with Oil Red O from different groups. **(D)**. Representative images and quantitative analysis of liver sections stained with Sirius Red from different groups.

group. Furthermore, the expression of p-NF- $\kappa$ B p65 protein in the LQAtta group was notably lower than that in the NASH group.

## Discussion

Over the past four decades, approximately 25% of adults worldwide have been diagnosed with NAFLD, a condition that has emerged as a primary contributor to liver cirrhosis and hepatocellular carcinoma. The incidence of this disease continues to rise annually.<sup>29,30</sup> NASH, a variant of NAFLD, is marked by necrotic inflammatory processes and rapid

**Table 4** NAS Scoring of H&E Images of Liver

Group	Steatosis	Lobular Inflammation	Hepatocyte Ballooning
Control	0	0	0
NASH	3	2	3
16 LQAtta	2	1	2
20 LQAtta	1	1	1

fibrosis development.<sup>4,31</sup> With the advancement of NAFLD, NASH may lead to the onset and exacerbation of hepatic fibrosis and cirrhosis. This progression highlights the urgent necessity for specific therapeutic strategies to efficiently manage NAFLD. Currently, there are no specific treatments available, and the clinical management of weight and fat reduction primarily involves dietary modifications along with increased physical activity. Nevertheless, to achieve a more comprehensive approach to treatment, the use of pharmacological agents is often necessary.<sup>4</sup> The quest for the development of safe and effective drugs that can postpone the progression of diseases has garnered significant interest in this field.<sup>32</sup> Studies have consistently shown that a variety of herbal treatments improve liver function in diseases such as NAFLD and NASH. Botanical formulations<sup>33–35</sup> have been demonstrated to effectively diminish lobular inflammation, fibrosis and reduce hepatic steatosis, and display strong antioxidant, anti-lipogenic properties, anti-apoptotic, and anti-inflammatory. For instance, a traditional Chinese herb called 919 syrup has been reported in the literature to effectively improve liver function in patients with non-alcoholic fatty liver disease (NAFLD) by inhibiting inflammatory

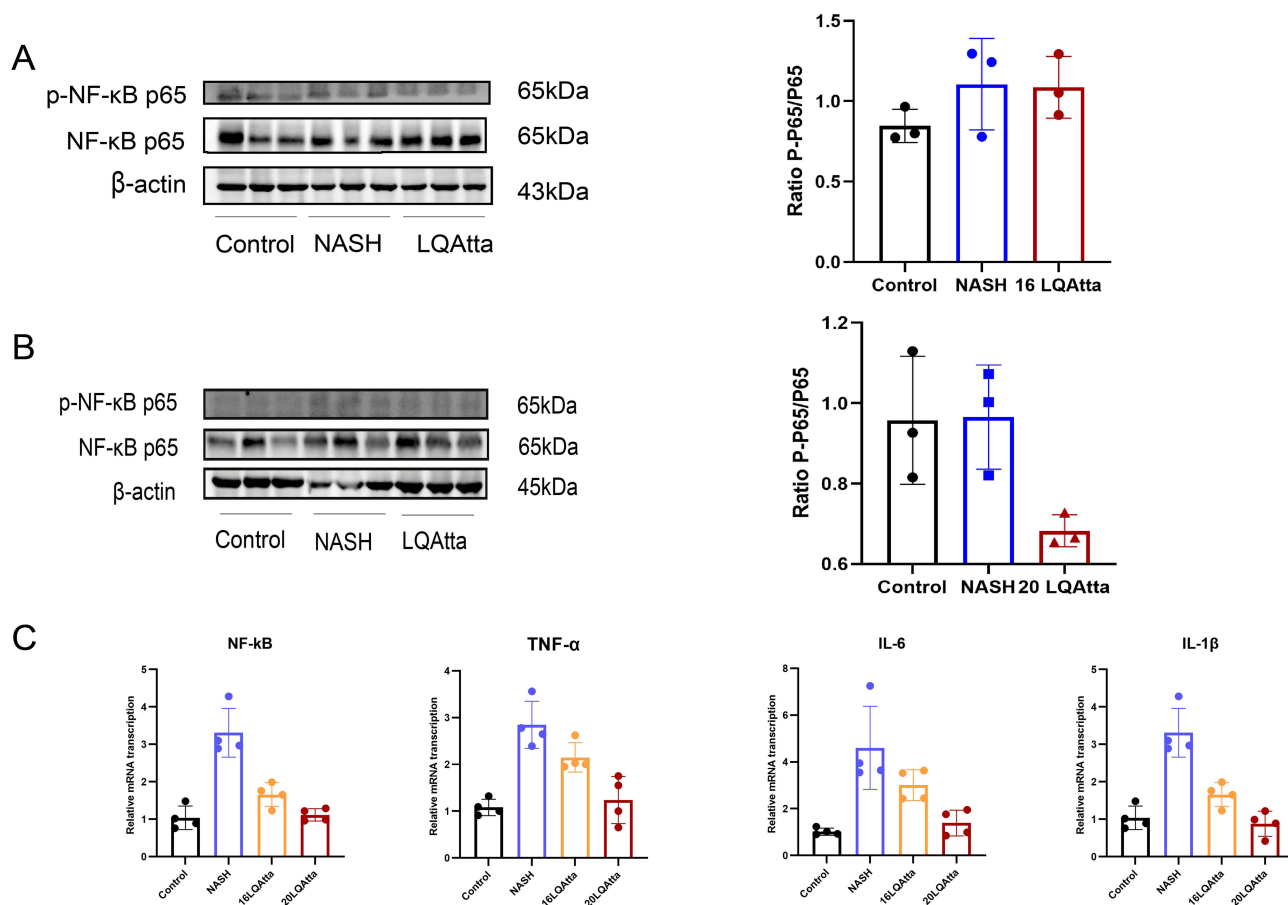


**Figure 5** LQAtta Potentially Regulates NASH via the NF-κB Pathway. **(A)** Western blot analysis and quantitative assessment of p-NF-κB p65 and NF-κB p65 protein levels in the 16-week LQAtta group. **(B)** Western blot analysis and quantitative assessment of p-NF-κB p65 and NF-κB p65 protein levels in the 20-week LQAtta group. **(C)** Relative mRNA levels of inflammation-related genes (TNF-α, IL-1β, IL-6) and NF-κB.

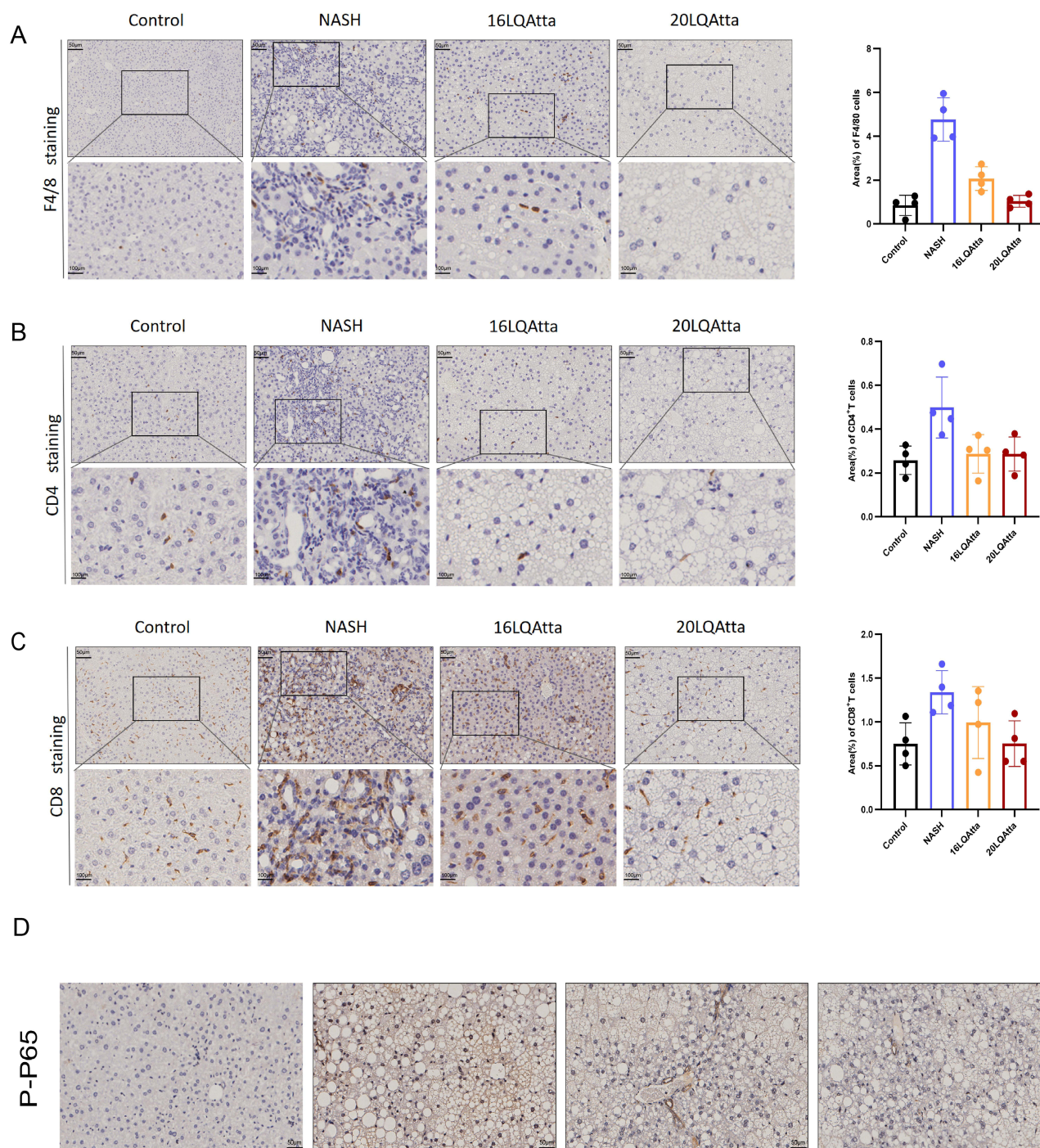


**Figure 6** Improvement of Immunohistochemical Levels in HFHC-Induced NASH Mice by LQAtta. **(A)**. Immunohistochemical sections and quantitative analysis of F4/80. **(B)**. Immunohistochemical sections and quantitative analysis of CD4. **(C)**. Immunohistochemical sections and quantitative analysis of CD8. **(D)**. Immunohistochemical sections within cell nuclei.

response and fat accumulation in the liver<sup>35</sup> Research unveiled the classic prescription of Kangxian ruangan capsule, which alleviated inflammatory responses, histopathological changes, and liver fibrosis in NAFLD fibrotic rats.<sup>33</sup> Another study revealed Cordycepin, a natural product with potent antioxidant and anti-inflammatory effects, that exerts significant protective effects against hepatic steatosis, inflammation, liver injury, and fibrosis in mice under metabolic stress through activation of the AMPK signaling pathway.<sup>36</sup> There's another piece of literature found that the water extract of *Curcuma longa* L. may ameliorate NAFLD by modulating fatty acid uptake.<sup>37</sup> Study demonstrated that Huanglian-Hongqu herb

ameliorates NAFLD by targeting the PPAR signaling pathway.<sup>38</sup> These plant-based treatments work by mitigating inflammatory processes in the liver, decreasing the accumulation of fat within liver cells, and preventing the formation of fibrous tissue. They provide significant antioxidant protection, reduce inflammation, inhibit cell death, and prevent lipid synthesis within the liver. Previous research<sup>18,19</sup> has shown that LQAtta offers substantial therapeutic advantages in treating liver cirrhosis and fibrosis.

The NASH model induced by an HFHC diet is both widely adopted and reproducible, demonstrating histopathological features in mice that closely resemble those observed in human NASH as reported in the source.<sup>39</sup> Nonetheless, the variability observed in the extent of steatosis, inflammation, and fibrosis presented by this model, coupled with its time-intensive nature, underscores the challenges of experimental consistency as noted in references.<sup>40,41</sup> The research conducted in this investigation has demonstrated a marked elevation in the serum concentrations of ALT, AST, and CHO in individuals diagnosed with NASH compared to the levels observed in participants belonging to the control group; the mouse livers were significantly enlarged, yellowish, slightly tough in texture, with blunt edges, and a greasy feel; and their histopathology showed steatosis, increased inflammation, and significantly increased infiltration of macrophages and immune cells. These findings indicate that the model group was successfully established.

Gross morphological changes in the liver are related to liver function.<sup>42</sup> Significant liver enlargement, yellowing, hepatocyte swelling, and balloon degeneration were observed in mice in the NASH model group. The histopathological changes induced by the HFHC diet in mice were reduced after LQAtta treatment. Findings from this investigation indicate that LQAtta exerts a hepatoprotective influence. LQAtta exerts its effects by soothing the liver. Metabolic syndrome, often identified by dyslipidemia, has a known association with NASH as evidenced by.<sup>43</sup> In this study, evaluations of liver function parameters alongside serum total cholesterol (CHO) demonstrated significant elevations in NASH-affected mice when compared with controls. Administration of LQAtta notably decreased serum CHO, AST, and ALT in liver tissue. Although no substantial differences in serum CHO were noted in the LQAtta group at the 16-week mark, significant reductions were observed after 20 weeks of treatment. The possible reason is that LQAtta, as a TCM compound preparation, has a slow onset, and the 16-week administration period was relatively short, not reaching the level of blood lipid-lowering treatment. This study suggests that the administration period of LQAtta may be 3 months. Because *n* of this study is less than 5, the results of this study are preliminary results and no statistical analysis has been conducted. In the future, the sample size will be further increased for research.

From the UHPLC-MS/MS analysis of LQAtta, a total of 1,518 chemical components were identified. These included 159 flavonoids, 92 terpenoids, 57 phenylpropanoids, 51 alkaloids, 46 compounds belonging to ketones, aldehydes, and acids, 38 phenols, 25 steroids, 21 amino acids, and 18 organic acids. Network pharmacology<sup>44</sup> serves as a comprehensive analytical tool that enables a systematic understanding of the therapeutic mechanisms of multi-component drugs. In this study, based on GO and KEGG enrichment analyses, multiple pathways closely related to the pathological processes of NASH were identified, such as the Toll-like receptor signaling pathway, the NF- $\kappa$ B signaling pathway, and inflammation-related pathways. Therefore, we speculate that the improvement effect of LQAtta on NASH may be closely related to its potent anti-inflammatory and antioxidant activities. Further experimental validation is required to elucidate its underlying mechanisms. Studies have indicated that NF- $\kappa$ B consists of a heterodimer formed by p50 and p65 subunits. Typically, NF- $\kappa$ B is associated with its inhibitor, I $\kappa$ B, creating an inactive trimer located within the cytoplasm.<sup>45–48</sup> Enhanced levels of phosphorylated p65 in NF- $\kappa$ B were detected in the hepatic tissues of NASH-affected mice via Western blot, as opposed to their healthy counterparts. Nonetheless, administration of LQAtta led to decreased levels of these proteins. Considering the pivotal involvement of the NF- $\kappa$ B pathway in the advancement of NASH, these observations suggest that LQAtta may effectively counteract disease progression in mice through the suppression of this signaling pathway. Liver inflammation is considered to be a major factor in the onset of NASH.<sup>49</sup> Cytokines are essential biomarkers of inflammation in NASH and this is why their levels are of importance.<sup>50</sup> In particular, TNF- $\alpha$  is a key cytokine involved in the development of NASH due to its strong relationship with the inflammatory processes modulated by the NF- $\kappa$ B pathway.<sup>51</sup> In this work, results show that TNF- $\alpha$ , IL-6, and IL-1 $\beta$  were significantly elevated in the liver tissue of patients with NASH as compared to the control group. After the administration of LQAtta, these cytokines were decreased to a certain extent. Thus, it may be concluded that LQAtta exerts anti-inflammatory effects through modulating the NF- $\kappa$ B activity and may have the potential for use in treating inflammation diseases.

In summary, based on the results of this study, it can be concluded that the NF- $\kappa$ B pathway may serve as a potential target for LQAtta in regulating the NASH animal model. Through metabolomics and network pharmacological screening, we have identified that LQAtta exerts its effects through multiple targets and pathways. Therefore, this study represents a preliminary experimental investigation, and further research is needed to explore other targets and clinical applications of LQAtta.

## Abbreviations

NAFLD, nonalcoholic fatty liver disease; NASH, nonalcoholic steatohepatitis; HFHC, high-fat/high-cholesterol; NF- $\kappa$ B, nuclear factor kappa-B; I $\kappa$ B, inhibitor of NF- $\kappa$ B; TNF- $\alpha$ , tumor necrosis factor- $\alpha$ ; IL-1 $\beta$ , Interleukin-1 $\beta$ ; IL-6, Interleukin-6 ALT, alanine aminotransferase; AST, aspartate aminotransferase; CHO, Serum total cholesterol; LQAtta, Lang Qing A ta.

## Data Sharing Statement

The data underlying this article will be shared on reasonable request to the corresponding author.

## Ethics Statements

All datasets in this study were downloaded from public databases. The current research follows database access policies and publication guidelines. According to item 1 and 2 of Article 32 of “the Measures for Ethical Review of Life Science and Medical Research Involving Human Subjects”, this study is exempt from ethical review and approval.

## Author Contributions

All authors made a significant contribution to the work reported, whether that is in the conception, study design, execution, acquisition of data, analysis and interpretation, or in all these areas; took part in drafting, revising or critically reviewing the article; gave final approval of the version to be published; have agreed on the journal to which the article has been submitted; and agree to be accountable for all aspects of the work.

## Funding

This study received financial support from the sixth “333 Talents” Outstanding Young Talents Project of Jiangsu Province (BRA2022013). All authors are very appreciative of the financial support.

## Disclosure

Shupe Li, Hanlong Zhu, Qi Zhai, Yu Hou, and Ya Yang are co-first authors for this study. There are no conflicts of interest to declare by the authors.

## References

- Chalasan N, Younossi Z, Lavine JE, et al. The diagnosis and management of nonalcoholic fatty liver disease: practice guidance from the American Association for the Study of Liver Diseases. *Hepatology*. 2018;67(1):328–357. doi:10.1002/hep.29367
- Deng Y-F, Xu -Q-Q, Chen T-Q, et al. Ginsenoside alleviates inflammation and fibrosis in experimental NASH mice by suppressing the NF- $\kappa$ B/NLRP3 signaling pathway. *Phytomedicine*. 2022;104:154241. doi:10.1016/j.phymed.2022.154241
- Han E, Lee B-W, Kang ES, et al. Mortality in metabolic dysfunction-associated steatotic liver disease: a nationwide population-based cohort study. *Metabolism*. 2024;152:155789. doi:10.1016/j.metabol.2024.155789
- Sheka AC, Adeyi O, Thompson J, Hameed B, Crawford PA, Ikramuddin S. Nonalcoholic Steatohepatitis: a Review. *JAMA*. 2020;323(12):1175–1183. doi:10.1001/jama.2020.2298
- Williams CD, Stengel J, Asike MI, et al. Prevalence of nonalcoholic fatty liver disease and nonalcoholic steatohepatitis among a largely middle-aged population utilizing ultrasound and liver biopsy: a prospective study. *Gastroenterology*. 2011;140(1):124–131. doi:10.1053/j.gastro.2010.09.038
- Charlton MR, Burns JM, Pedersen RA, Watt KD, Heimbach JK, Dierkhising RA. Frequency and outcomes of liver transplantation for nonalcoholic steatohepatitis in the United States. *Gastroenterology*. 2011;141(4):1249–1253. doi:10.1053/j.gastro.2011.06.061
- Majeed M, Majeed S, Nagabhushanam K, Lawrence L, Mundkur L. Novel combinatorial regimen of garcinol and curcuminoids for Non-alcoholic Steatohepatitis (NASH) in Mice. *Sci Rep*. 2020;10(1):7440. doi:10.1038/s41598-020-64293-w
- Angulo P, Kleiner DE, Dam-Larsen S, et al. Liver fibrosis, but no other histologic features, is associated with long-term outcomes of patients with nonalcoholic fatty liver disease. *Gastroenterology*. 2015;149(2):389–397.e10. doi:10.1053/j.gastro.2015.04.043

9. Ekstedt M, Hagström H, Nasr P, et al. Fibrosis stage is the strongest predictor for disease-specific mortality in NAFLD after up to 33 years of follow-up. *Hepatology*. 2015;61(5):1547–1554. doi:10.1002/hep.27368
10. Zhu H, Zhao T, Zhao S, et al. O-GlcNAcylation promotes the progression of nonalcoholic fatty liver disease by upregulating the expression and function of CD36. *Metabolism*. 2024;156:155914. doi:10.1016/j.metabol.2024.155914
11. Gerry AB, Leake DS. Effect of low extracellular pH on NF- $\kappa$ B activation in macrophages. *Atherosclerosis*. 2014;233(2):537–544. doi:10.1016/j.atherosclerosis.2014.01.014
12. Ghosh S, Karin M. Missing pieces in the NF-kappaB puzzle. *Cell*. 2002;109:S81–S96. doi:10.1016/S0092-8674(02)00703-1
13. Heida A, Gruben N, Catrysse L, et al. The hepatocyte IKK:NF- $\kappa$ B axis promotes liver steatosis by stimulating de novo lipogenesis and cholesterol synthesis. *mol Metab*. 2021;54:101349. doi:10.1016/j.molmet.2021.101349
14. Bartuzi P, Hofker MH, van de Sluis B. Tuning NF- $\kappa$ B activity: a touch of COMMD proteins. *Biochim Biophys Acta*. 2013;1832(12):2315–2321. doi:10.1016/j.bbadis.2013.09.014
15. Xu S, Deng K-Q, Lu C, et al. Interleukin-6 classic and trans-signaling utilize glucose metabolism reprogramming to achieve anti- or pro-inflammatory effects. *Metabolism*. 2024;155:155832. doi:10.1016/j.metabol.2024.155832
16. Farrell GC, van Rooyen D, Gan L, Chitturi S. NASH is an inflammatory disorder: pathogenic, prognostic and therapeutic implications. *Gut Liver*. 2012;6(2):149–171. doi:10.5009/gnl.2012.6.2.149
17. Aoyama Y, Naiki-Ito A, Xiaochen K, et al. Lactoferrin prevents hepatic injury and fibrosis via the inhibition of NF- $\kappa$ B signaling in a rat non-alcoholic steatohepatitis model. *Nutrients*. 2021;14(1):42. doi:10.3390/nu14010042
18. Xuan J, Wen W, Wang Y, et al. Effect of Huangtongluofang, a Chinese traditional medicine, in hepatic fibrogenesis in a mouse model of biliary cirrhosis. *Cell Physiol Biochem*. 2017;44(1):368–376. doi:10.1159/000484908
19. Xuan J, Huang A, Hu D, et al. Huang tongluo Fang improves liver fibrosis via down-regulating miR-184 and up-regulating FOXO1 to inhibit Th17 cell differentiation. *Exp Mol Pathol*. 2020;115:104447. doi:10.1016/j.yexmp.2020.104447
20. Johnson CH, Ivanisevic J, Siuzdak G. Metabolomics: beyond biomarkers and towards mechanisms. *Nat Rev Mol Cell Biol*. 2016;17(7):451–459. doi:10.1038/nrm.2016.25
21. Wu -S-S, Xu -X-X, Shi -Y-Y, et al. System pharmacology analysis to decipher the effect and mechanism of active ingredients combination from herb couple on rheumatoid arthritis in rats. *J Ethnopharmacol*. 2022;288:114969. doi:10.1016/j.jep.2022.114969
22. Zhao L, Zhang H, Li N, et al. Network pharmacology, a promising approach to reveal the pharmacology mechanism of Chinese medicine formula. *J Ethnopharmacol*. 2023;309:116306. doi:10.1016/j.jep.2023.116306
23. Zhao Y, Xi C, Liu D, et al. Chemical components with antibacterial properties found in sanchen powder from traditional Tibetan medicine. *J Ethnopharmacol*. 2024;326:117981. doi:10.1016/j.jep.2024.117981
24. Vasilev N, Bocard J, Lang G, et al. Structured plant metabolomics for the simultaneous exploration of multiple factors. *Sci Rep*. 2016;6:37390. doi:10.1038/srep37390
25. Demurtas A, Pescina S, Nicoli S, Santi P, Ribeiro de Araujo D, Padula C. Validation of a HPLC-UV method for the quantification of budesonide in skin layers. *J Chromatogr B Analyt Technol Biomed Life Sci*. 2021;1164:122512. doi:10.1016/j.jchromb.2020.122512
26. Zelena E, Dunn WB, Broadhurst D, et al. Development of a robust and repeatable UPLC-MS method for the long-term metabolomic study of human serum. *Anal Chem*. 2009;81(4):1357–1364. doi:10.1021/ac8019366
27. Want EJ, Masson P, Michopoulos F, et al. Global metabolic profiling of animal and human tissues via UPLC-MS. *Nat Protoc*. 2013;8(1):17–32. doi:10.1038/nprot.2012.135
28. Colosimo S, Miller H, Koutoukidis DA, et al. Glycated haemoglobin is a major predictor of disease severity in patients with NAFLD. *Diabetes Res Clin Pract*. 2024;217:111820. doi:10.1016/j.diabres.2024.111820
29. Wang X, Tanaka N, Hu X, et al. A high-cholesterol diet promotes steatohepatitis and liver tumorigenesis in HCV core gene transgenic mice. *Arch Toxicol*. 2019;93(6):1713–1725. doi:10.1007/s00204-019-02440-7
30. Powell EE, Wong VW-S, Rinella M. Non-alcoholic fatty liver disease. *Lancet*. 2021;397(10290):2212–2224. doi:10.1016/S0140-6736(20)32511-3
31. Wang X, Wang L, Geng L, Tanaka N, Ye B. Resmetirom ameliorates NASH-model mice by suppressing STAT3 and NF- $\kappa$ B signaling pathways in an RGS5-dependent manner. *Int J Mol Sci*. 2023;24(6). doi:10.3390/ijms24065843
32. Lv S, Zhang Z, Su X, et al. Qingrequzhuo capsule alleviated methionine and choline deficient diet-induced nonalcoholic steatohepatitis in mice through regulating gut microbiota, enhancing gut tight junction and inhibiting the activation of TLR4/NF- $\kappa$ B signaling pathway. *Front Endocrinol*. 2022;13:1106875. doi:10.3389/fendo.2022.1106875
33. Liu L, Zhou Y, Dai D, Xia H, Zhao K, Zhang J. Protective effects of Kangxian ruangan capsule against nonalcoholic fatty liver disease fibrosis in rats induced by MCD diet. *Biomed Pharmacother*. 2018;108:424–434. doi:10.1016/j.biopha.2018.06.134
34. Zhang L, Yao Z, Ji G. Herbal extracts and natural products in alleviating non-alcoholic fatty liver disease via activating autophagy. *Front Pharmacol*. 2018;9:1459. doi:10.3389/fphar.2018.01459
35. Chen M, Xing J, Pan D, Peng X, Gao P. Chinese herbal medicine mixture 919 syrup alleviates nonalcoholic fatty liver disease in rats by inhibiting the NF- $\kappa$ B pathway. *Biomed Pharmacother*. 2020;128:110286. doi:10.1016/j.biopha.2020.110286
36. Lan T, Yu Y, Zhang J, et al. cordycepin ameliorates nonalcoholic steatohepatitis by activation of the AMP-activated protein kinase signaling pathway. *Hepatology*. 2021;74(2):686–703. doi:10.1002/hep.31749
37. Mun J, Kim S, Yoon H-G, et al. Water extract of Curcuma longa L. Ameliorates non-alcoholic fatty liver disease. *Nutrients*. 2019;11(10):2536. doi:10.3390/nu11102536
38. Zhang X, Zhang J, Zhou Z, et al. Integrated network pharmacology, metabolomics, and transcriptomics of Huanglian-Hongqu herb pair in non-alcoholic fatty liver disease. *J Ethnopharmacol*. 2024;325:117828. doi:10.1016/j.jep.2024.117828
39. Santhekadur PK, Kumar DP, Sanyal AJ. Preclinical models of non-alcoholic fatty liver disease. *J Hepatol*. 2018;68(2):230–237. doi:10.1016/j.jhep.2017.10.031
40. Takahashi Y, Soejima Y, Fukusato T. Animal models of nonalcoholic fatty liver disease/nonalcoholic steatohepatitis. *World J Gastroenterol*. 2012;18(19):2300–2308. doi:10.3748/wjg.v18.i19.2300
41. Zhang T, Hu J, Wang X, et al. MicroRNA-378 promotes hepatic inflammation and fibrosis via modulation of the NF- $\kappa$ B-TNF $\alpha$  pathway. *J Hepatol*. 2019;70(1):87–96. doi:10.1016/j.jhep.2018.08.026

42. Yang J-M, Sun Y, Wang M, et al. Regulatory effect of a Chinese herbal medicine formula on non-alcoholic fatty liver disease. *World J Gastroenterol.* 2019;25(34):5105–5119. doi:10.3748/wjg.v25.i34.5105
43. Tsai -C-C, Lin Y-J, Yu H-R, et al. Melatonin alleviates liver steatosis induced by prenatal dexamethasone exposure and postnatal high-fat diet. *Exp Ther Med.* 2018;16(2):917–924. doi:10.3892/etm.2018.6256
44. Qiu P, Mi A, Hong C, et al. An integrated network pharmacology approach reveals that *Ampelopsis grossedentata* improves alcoholic liver disease via TLR4/NF- $\kappa$ B/MLKL pathway. *Phytomedicine.* 2024;132:155658. doi:10.1016/j.phymed.2024.155658
45. Saha M, Manna K, Das saha K. Melatonin suppresses NLRP3 inflammasome activation via TLR4/NF- $\kappa$ B and P2X7R signaling in high-fat diet-induced Murine NASH Model. *J Inflamm Res.* 2022;15:3235–3258. doi:10.2147/JIR.S343236
46. Liu Y-L, Zhang Q-Z, Wang Y-R, et al. Astragaloside IV improves high-fat diet-induced hepatic steatosis in nonalcoholic fatty liver disease rats by regulating inflammatory factors level via TLR4/NF- $\kappa$ B signaling pathway. *Front Pharmacol.* 2020;11:605064. doi:10.3389/fphar.2020.605064
47. Li R, Li J, Huang Y, et al. Polydatin attenuates diet-induced nonalcoholic steatohepatitis and fibrosis in mice. *Int J Biol Sci.* 2018;14(11):1411–1425. doi:10.7150/ijbs.26086
48. Wang X, de Carvalho Ribeiro M, Iracheta-Vellve A, et al. Macrophage-specific hypoxia-inducible factor-1 $\alpha$  contributes to impaired autophagic flux in nonalcoholic steatohepatitis. *Hepatology.* 2019;69(2):545–563. doi:10.1002/hep.30215
49. Wree A, Broderick L, Canbay A, Hoffman HM, Feldstein AE. From NAFLD to NASH to cirrhosis-new insights into disease mechanisms. *Nat Rev Gastroenterol Hepatol.* 2013;10(11):627–636. doi:10.1038/nrgastro.2013.149
50. Mridha AR, Wree A, Robertson AAB, et al. NLRP3 inflammasome blockade reduces liver inflammation and fibrosis in experimental NASH in mice. *J Hepatol.* 2017;66(5):1037–1046. doi:10.1016/j.jhep.2017.01.022
51. Méndez-Sánchez N, Valencia-Rodríguez A, Coronel-Castillo C, et al. The cellular pathways of liver fibrosis in non-alcoholic steatohepatitis. *Ann Transl Med.* 2020;8(6):400. doi:10.21037/atm.2020.02.184

## Drug Design, Development and Therapy

### Publish your work in this journal

Drug Design, Development and Therapy is an international, peer-reviewed open-access journal that spans the spectrum of drug design and development through to clinical applications. Clinical outcomes, patient safety, and programs for the development and effective, safe, and sustained use of medicines are a feature of the journal, which has also been accepted for indexing on PubMed Central. The manuscript management system is completely online and includes a very quick and fair peer-review system, which is all easy to use. Visit <http://www.dovepress.com/testimonials.php> to read real quotes from published authors.

Submit your manuscript here: <https://www.dovepress.com/drug-design-development-and-therapy-journal>

**Dovepress**  
Taylor & Francis Group